Amino Acids (2014) 46:2721–2732
DOI 10.1007/s00726-014-1828-6

ORIGINAL ARTICLE

In vivo NIRF imaging-guided delivery of a novel NGR–VEGI fusion protein for targeting tumor vasculature

Wenhui Ma · Guoquan Li · Jing Wang · Weidong Yang · Yingqi Zhang · Peter S. Conti · Kai Chen

Received: 16 May 2014 / Accepted: 17 August 2014 / Published online: 3 September 2014

Abstract Pathological angiogenesis is crucial in tumor growth, invasion and metastasis. Previous studies demonstrated that the vascular endothelial growth inhibitor (VEGI), a member of the tumor necrosis factor superfamily, can be used as a potent endogenous inhibitor of tumor angiogenesis. Molecular probes containing the asparagine–glycine–arginine (NGR) sequence can specifically bind to CD13 receptor which is overexpressed on neovasculature and several tumor cells. Near-infrared fluorescence (NIRF) optical imaging for targeting tumor vasculature offers a noninvasive method for early detection of tumor angiogenesis and efficient monitoring of response to anti-tumor vasculature therapy. The aim of this study was to develop a new NIRF imaging probe on the basis of an NGR–VEGI protein for the visualization of tumor vasculature. The NGR–VEGI fusion protein was prepared from prokaryotic expression, and its function was characterized in vitro. The NGR–VEGI protein was then labeled with a Cy5.5 fluorophore to afford Cy5.5-NGR–VEGI probe. Using the NIRF imaging technique, we visualized and quantified the specific delivery of Cy5.5-NGR–VEGI protein to subcutaneous HT-1080 fibrosarcoma tumors in mouse xenografts. The Cy5.5-NGR–VEGI probe exhibited rapid HT-1080 tumor targeting, and highest tumor-to-background contrast at 8 h post-injection (pi). Tumor specificity of Cy5.5-NGR–VEGI was confirmed by effective blocking of tumor uptake in the presence of unlabeled NGR–VEGI (20 mg/kg). Ex vivo NIRF imaging further confirmed in vivo imaging findings, demonstrating that Cy5.5-NGR–VEGI displayed an excellent tumor-to-muscle ratio (18.93 ± 2.88) at 8 h pi for the non-blocking group and significantly reduced ratio (4.92 ± 0.75) for the blocking group. In conclusion, Cy5.5-NGR–VEGI provided highly sensitive, target-specific, and longitudinal imaging of HT-1080 tumors. As a novel theranostic protein, Cy5.5-NGR–VEGI has the potential to improve cancer treatment by targeting tumor vasculature.

Keywords NIRF imaging · Tumor vasculature · CD13 receptor · NGR · Vascular endothelial growth inhibitor

Abbreviations

NIRF	Near-infrared fluorescence
VEGI	Vascular endothelial growth inhibitor
TNF	Tumor necrosis factor
NGR	Asparagine-glycine-arginine
APN	Aminopeptidase N
TNF-α	Tumor necrosis factor-alpha
IFN	Interferon
DOX	Doxorubicin
NHS	*N*-hydroxysuccinimide
DMSO	Dimethyl sulfoxide
HUVEC	Human umbilical vein endothelial cell line
DMEM	Dulbecco's Modified Eagle's Medium

W. Ma and G. Li contributed equally to this work.

W. Ma · G. Li · P. S. Conti · K. Chen (✉)
Department of Radiology, Molecular Imaging Center, Keck School of Medicine, University of Southern California, 2250 Alcazar Street, CSC 103, Los Angeles, CA 90033-9061, USA
e-mail: chenkai@usc.edu

W. Ma · G. Li · J. Wang (✉) · W. Yang
Department of Nuclear Medicine, Xijing Hospital, The Fourth Military Medical University, Xi'an, Shaanxi 710032, People's Republic of China
e-mail: wangjing@fmmu.edu.cn

Y. Zhang
State Key Laboratory of Cancer Biology, Department of Biopharmaceutics, School of Pharmacy, The Fourth Military Medical University, Xi'an, Shaanxi 710032, People's Republic of China

FBS	Fetal bovine serum
PBS	Phosphate-buffered saline
PFA	Paraformaldehyde
DAPI	4′,6-Diamidino-2-phenylindole
pi	Post-injection
ROIs	Regions of interest

Introduction

Angiogenesis is a biological process through which new capillaries sprout from existing blood vessels (Goncalves et al. 2005). In an adult, physiological angiogenesis only occurs in the female reproduction or during episodes of wound healing (Risau 1997). In contrast, pathological angiogenesis is usually associated with numerous disease states, including inflammation, vascular retinopathy, rheumatoid arthritis and cancer (Balkwill et al. 2005; Carmeliet 2005; Coussens and Werb 2002; Hanahan and Folkman 1996; Lopez-Otin and Matrisian 2007). Over the past decades, numerous anti-angiogenic agents with diverse mechanisms of action have been developed for targeting tumor angiogenesis (Folkman 1971, 2006). Among these anti-angiogenic agents, vascular endothelial growth inhibitor (VEGI) has attracted significant research interest (Duan et al. 2012; Zhang et al. 2009a). VEGI is a member of the TNF superfamily (TNFSF15), which has been identified as an endothelial cell-specific gene and a potent endogenous inhibitor of endothelial cell proliferation, angiogenesis and tumor growth (Zhang et al. 2009a). Previous reports demonstrated that the recombinant human VEGI-174 remarkably suppresses the tumor cell growth by targeting angiogenesis in vitro as well as in tumor-bearing animal models (Zhai et al. 1999a, b). Additional studies showed that VEGI could inhibit the growth of epithelial cells and various tumor cells, including human epithelial carcinoma, human histiocytic lymphoma U-937, human breast carcinoma MCF-7, murine colon cancer cells MC-38, and human myeloid lymphoma ML-1a (Haridas et al. 1999; Parr et al. 2006; Xiao et al. 2005). The power of VEGI for tumor cell inhibition was further demonstrated on the motility and adhesion of bladder cancer cells and prostate cancer cells (Zhang et al. 2010, 2009b). In a clinical study, Parr et al. found that breast cancer patients with reduced levels of VEGI had higher local recurrence, shorter survival time, and poorer prognosis than those with high levels of VEGI (Parr et al. 2006). Therefore, VEGI was considered as one of the most promising anticancer agents by suppressing neovascularization. However, the limited source of natural VEGI hampers its translation into clinical studies, leading to an alternative approach by generating the analogs of recombinant VEGI (Duan et al. 2012).

While the application of recombinant VEGI showed the promise for cancer therapy, most of new VEGI analogs suffer from low tumor specificity, causing adverse side effects (Duan et al. 2012). CD13 receptor, also named as aminopeptidase N (APN), is a zinc dependent membrane-bound ectopeptidase, which has been identified as a critical regulator of angiogenesis (Bhagwat et al. 2001) where its expression on activated blood vessels is induced by angiogenic signals (Guzman-Rojas et al. 2012). We and others have showed that the peptide or protein containing the asparagine-glycine-arginine (NGR) sequence can specifically bind to tumors where the overexpression of CD13 receptor was identified (Petrovic et al. 2007; Pasqualini et al. 2000; von Wallbrunn et al. 2008; Westphal et al. 2013; Zhang et al. 2005). Some elegant studies also showed that anticancer drugs, such as tumor necrosis factor-alpha (TNF-α), interferon (IFN), and doxorubicin (DOX), after conjugation with the NGR motif, could be precisely delivered to neoangiogenic sites for tumor imaging and therapy (Chen et al. 2013; Meng et al. 2007; Sacchi et al. 2004; Westphal et al. 2013). Taken together, we hypothesize that an approach which combines VEGI with CD13-targeted NGR sequence may improve the tumor specificity of VEGI, and offer a novel biomaterial for targeting tumor vasculature.

The molecular medicine revolution is being enabled by molecular imaging, which is making cancer treatment more predictive, personalized, and responsive. In the past decade, significant advances have been made in the field of cancer molecular imaging for both preclinical and clinical research (Weissleder 2006). The beauty of molecular imaging techniques comes from their intrinsic capabilities to noninvasively visualize, characterize, and measure the changes of biological functions associated with disease progression at the molecular and cellular levels (Chen and Conti 2010; Chen and Chen 2010, 2011; Xing et al. 2014). Anticancer agents after appropriate conjugation with imaging moieties (Chen and Chen 2010) can be utilized as theranostics, combining both therapeutic and diagnostic capabilities in one dose, which has the potential to overcome undesirable differences in biodistribution and selectivity that currently exist between distinct imaging and therapeutic agents (Kelkar and Reineke 2011). Consequently, the theranostic agents may open up new opportunities to image and monitor the diseased tissue, delivery kinetics, and drug efficacy with the long-term expectation to ultimately optimize the treatment plan.

The specific aims of this study are to (1) prepare an NGR–VEGI fusion protein from prokaryotic expression, (2) characterize the in vitro function of the NGR–VEGI protein, (3) conjugate the NGR–VEGI protein with a Cy5.5 fluorophore, and (4) evaluate tumor-targeting efficacy and pharmacokinetics of the resulting Cy5.5-NGR–VEGI probe (Fig. 1) in tumor-bearing mice. Using the NIRF imaging

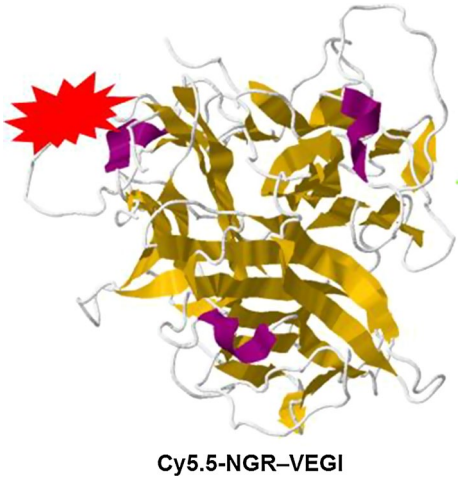

Fig. 1 Schematic structure of the Cy5.5-NGR–VEGI fusion protein

technique, the in vivo specific delivery of Cy5.5-NGR–VEGI protein to HT-1080 tumors in mouse xenografts was visualized and quantified.

Materials and methods

General

All chemicals (reagent grade) were obtained from commercial suppliers and used without further purification. The monomeric NGR peptide [C*NGR*C; disulfide Cys:Cys = 1–5] was purchased from C S Bio, Inc. (Menlo Park, CA, USA). The bacterial culture reagents and antibiotics were obtained from the Sangon Biotech (Shanghai, China). Cy5.5 monofunctional NHS ester (Cy5.5-NHS) and PD-10 column were purchased from GE Healthcare (Piscataway, NJ, USA).

Production of NGR–VEGI fusion protein

The NGR–VEGI expressed plasmid pET28a-NGR–VEGI was constructed according to a procedure described previously (Studier 2005). In brief, the cDNA coding region for NGR–VEGI (human VEGI fused with the *N* terminus of C*NGR*CVSGCAGRC motif) was obtained by PCR engineering of a plasmid containing the VEGI cDNA sequence, using the following primers: 5′-ACCATATG GTATACA CGTTGCCG-3′ (5′primer); 5′-GTCTCGAGTTAGAGCAG AAACGC-3′ (3′primer). The primer sequences were designed to include the NdeI and XhoI restriction sites for PCR cloning into a prokaryotic expression vector pET28a (Novagen, Darmstadt, Germany). The purification of NGR–VEGI protein was performed according to a standard method (Biomics Biotechnologies Co., Jiangsu, China) using a combination of Origami B (DE3) strain, autoinduction expression system, and affinity chromatography. The purified NGR–VEGI protein was examined using reducing SDS–PAGE (12 % separation gel).

Labeling of NGR–VEGI with Cy5.5 fluorophore

NGR–VEGI (0.5 mg, 0.024 μmol) was dissolved in 150 μL of sodium borate buffer (0.02 M, pH 8.5) and mixed with Cy5.5-NHS (0.027 mg, 0.024 μmol) in 5 μL of DMSO. The mixture was stirred at room temperature in the dark for 2 h, and then purified by PD-10 column. The desired Cy5.5-NGR–VEGI protein was collected, lyophilized, and stored at −20 °C in the dark until use (0.45 mg, yield: 86 %).

Cell line and culture condition

Human fibrosarcoma cell line (HT-1080) and human umbilical vein endothelial cell line (HUVEC) were obtained from the American Type Culture Collection (ATCC, Manassas, VA, USA). HT-1080 and HUVEC cells were grown in Dulbecco's Modified Eagle's Medium (DMEM) (USC Cell Culture Core, Los Angeles, CA, USA) supplemented with 10 % fetal bovine serum (FBS), penicillin and streptomycin (100 U/mL) at 37 °C in humidified atmosphere containing 5 % CO_2.

Flow cytometry

HUVEC was seeded in 60 mm plates at a density of 2.0×10^5 cells per well 24 h prior to the experiment. The cells were then incubated for 12 h with vector control, NGR peptide (20 nM), VEGI protein (20 nM), and purified NGR-VEGI protein (20 nM), respectively. After washing with phosphate-buffered saline (PBS) three times, the cells were incubated with 500 μL of binding buffer containing FITC-Annexin V and propidium iodide (PI) in the dark for 15 min at room temperature, according to the manufacturer's instructions (Beyotime Co., Shanghai, China). The cells were analyzed by a flow cytometer (FACSCalibur flow cytometer, Becton–Dickinson, San Jose, CA, USA) using a double FITC-Annexin V/PI staining approach.

Absorption and emission spectra

The absorption spectrum of Cy5.5-NGR–VEGI protein was recorded on a Cary 14 UV–Vis spectrometer (Bogart, GA, USA). The spectrum was scanned from 550 to 800 nm with an increment of 1 nm. The fluorescence emission of Cy5.5-NGR–VEGI was measured using a Shimadzu RF-5301PC spectrofluorophotometer (Columbia, MD, USA), and the spectrum was scanned from 550 to 800 nm with an

increment of 1 nm. The wavelength of excitation light was set at 650 nm.

In vitro fluorescence imaging of Cy5.5-NGR–VEGI

HT-1080 cells were grown in chamber slides (VWR Corporate, Radnor, PA, USA) with a density of 5×10^4/well for 24 h. After washing with serum-free DMEM medium for 3 min, the cells in each well were fixed with 4 % paraformaldehyde (PFA) for 10 min, and then washed with serum-free DMEM medium (3 times, 3 min/wash). The HT-1080 cells were incubated with 2 μM of Cy5.5-NGR–VEGI protein in 200 μL of serum-free DMEM medium at 37 °C in the dark for 30 min, followed by the PBS wash (3 times, 5 min/wash). For the blocking group, the HT-1080 cells were co-incubated with 2 μM of Cy5.5-NGR–VEGI protein and 2 mM of unlabeled NGR peptide. The chamber slides were then mounted with a DAPI (4′,6-diamidino-2-phenylindole) containing mounting medium, and placed under a Zeiss LSM 510 confocal laser scanning microscope (Carl Zeiss Microscopy, LLC, Thornwood, NY, USA).

Animal model

All animal procedures were performed according to a protocol approved by University of Southern California Institutional Animal Care and Use Committee. Female athymic nude mice (about 4–6 weeks old, with a body weight of 20–25 g) were obtained from Harlan Laboratories (Livermore, CA, USA). The HT-1080 tumor xenografts were generated by subcutaneous injection of 5×10^6 HT-1080 cells suspended in 50 μL of cell culture media and 50 μL of BD Matrigel (BD Biosciences, San Jose, CA, USA) into the right shoulder of mice. The cells were allowed to grow 2 weeks until tumors were 200–300 mm^3 in volume. Tumor growth was measured using caliper measurements in orthogonal dimensions.

In vivo and ex vivo NIRF imaging

In vivo fluorescence imaging was performed using the IVIS Imaging System 200 Series and analyzed using the IVIS Living Imaging 4.4 software (PerkinElmer Inc., Alameda, CA, USA). A Cy5.5 filter set was used to acquire the fluorescence of Cy5.5-NGR–VEGI protein. Identical illumination settings (lamp voltage, filters, f/stop, field of views, binning) were used to acquire all images. Fluorescence emission images were normalized and reported as photons per second per centimeter squared per steradian (p/s/cm^2/sr). The mice in the non-blocking group ($n = 6$) received 1.5 nmol of Cy5.5-NGR–VEGI intravenously and subjected to optical imaging at various time points post-injection (pi). The mice in the blocking group ($n = 6$) were injected with a mixture of Cy5.5-NGR–VEGI (1.5 nmol) and NGR–VEGI protein (20 mg/kg). All near-infrared fluorescence images were acquired using 1 s exposure time (f/stop = 4). Animals were anesthetized by inhalation of 2 % isoflurane during NIRF imaging. Mice from the non-blocking group ($n = 3$) and the blocking group ($n = 3$) were euthanized at 8 h pi. The tumors, tissues, and organs were dissected and subjected to ex vivo fluorescence imaging. Fluorescence intensities of tumor and organs were quantified using regions of interest (ROIs) that encompassed the entire organ. The mean fluorescence for each sample was reported.

Statistical analysis

All the data were presented as mean ± standard deviation (SD) of n independent measurements. Statistical analysis was performed with a Student's t test. Statistical significance was assigned for P values <0.05. To determine tumor contrast, mean fluorescence intensities of the tumor (T) area at the right shoulder of the animal and of the normal tissue (N) at the surrounding tissue were calculated using the region-of-interest (ROI) function of the IVIS Living Image 4.4 software. Dividing T by N yielded the contrast between tumor and normal tissue.

Results

Production and characterization of NGR–VEGI fusion protein

The NGR–VEGI fusion protein was successfully prepared through a protein expression system using Origami B (DE3) host strains. The reducing SDS-PAGE results showed that the NGR–VEGI protein expression cannot be identified without IPTG induction (Fig. 2, Lane 2), whereas a high yield of NGR–VEGI protein expression can be induced with 0.5 mM of isopropyl β-*D*-1-thiogalactopyranoside (IPTG) at 37 °C for 4 h (Fig. 2, Lane 3). A predominant NGR–VEGI fusion protein with a total of 186 amino acids was detected as a single band (corresponding to the expected molecular weight =21 kDa). The subsequent purification can be achieved with a high degree of purity for the target NGR–VEGI fusion protein (Fig. 2, Lane 4).

Flow cytometry analysis of cell apoptosis induced by NGR–VEGI protein

The inhibitory effect on the growth of HUVEC cells by NGR–VEGI protein was determined using flow cytometry analysis with a double FITC-Annexin V/PI staining

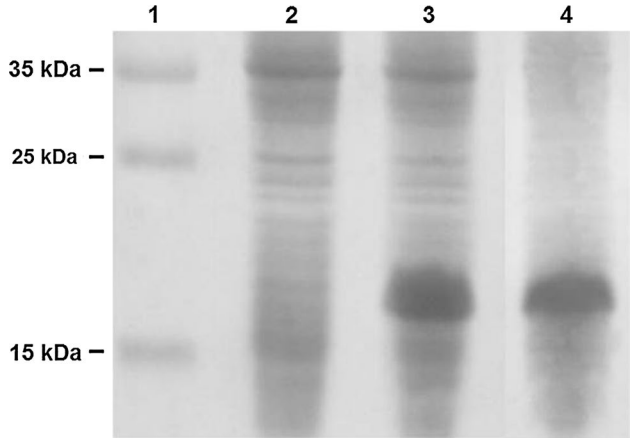

Fig. 2 SDS-PAGE analysis of NGR–VEGI fusion protein, showing NGR–VEGI expression is dependent on the IPTG induction. Lane 1: Molecular weight markers. Lane 2: Induction without IPTG. Lane 3: Induction with IPTG, expected MW = 21 kDa. Lane 4: purified NGR–VEGI fusion protein, expected MW = 21 kDa

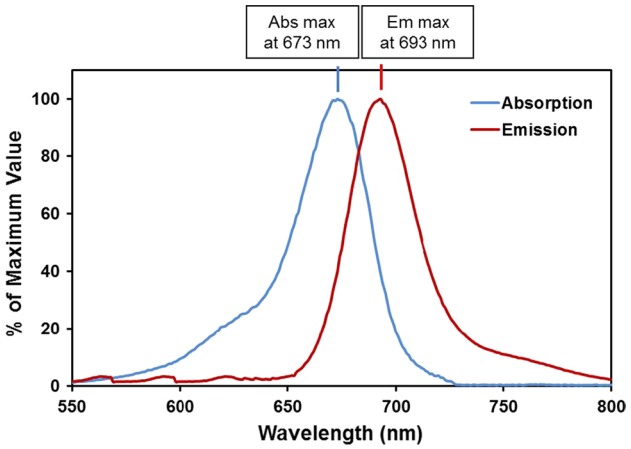

Fig. 4 Absorption and emission fluorescence spectra of Cy5.5-NGR–VEGI fusion protein

approach. Following treatment with vector control, NGR peptide (20 nM), VEGI protein (20 nM), and NGR–VEGI protein (20 nM), respectively, in proliferating HUVEC, the apoptotic HUVEC population was sorted out as indicated by the FITC-Annexin V positive staining. As shown in Fig. 3, the endothelial apoptosis induced by the NGR–VEGI protein (24.21 %) was significantly higher than that induced by the vector control (1.13 %) or NGR peptide (2.91 %), and larger than that induced by the VEGI protein only (22.54 %). The data suggested that the NGR–VEGI fusion protein produced from the IPTG induction expression system capitalizes the functionality of VEGI protein.

Spectrofluorophotometer of Cy5.5-NGR–VEGI

The absorption and fluorescence emission spectra of the Cy5.5-NGR–VEGI protein are shown in Fig. 4. The maximum absorption and fluorescence emission wavelength of the Cy5.5-NGR–VEGI was determined to be 673 and 693 nm, respectively.

Binding specificity of Cy5.5-NGR–VEGI

To determine the CD13 binding specificity and subcellular localization of Cy5.5-NGR–VEGI, the probe was incubated with CD13-positive HT-1080 tumor cells, and laser confocal microscopic imaging was carried out after 30 min incubation at 37 °C. Intensive fluorescent signal was observed from the membrane of HT-1080 cells, and some fluorescent signals were also found to be in the cytoplasm of the cells (Fig. 5, top). In addition, the fluorescent signal from the cells could be significantly reduced by incubation of the HT-1080 cells with large excess of the unlabeled NGR–VEGI protein (Fig. 5, bottom), indicating that Cy5.5-NGR–VEGI specifically binds to CD13 receptor.

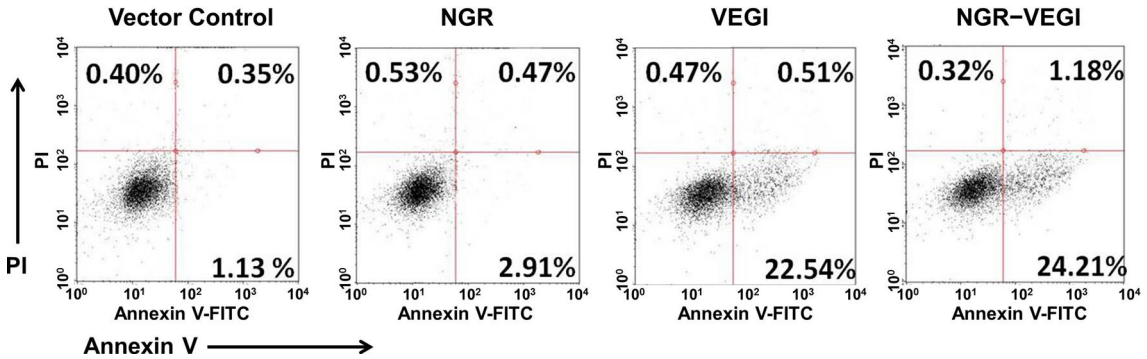

Fig. 3 Flow cytometry analysis of apoptosis induced by purified NGR–VEGI protein (20 nM) in proliferating HUVEC as compared to vector control, NGR peptide (20 nM), and VEGI protein (20 nM). Double FITC-Annexin V/PI negative cells indicate the live cell population, whereas FITC-Annexin V positive cells indicate the apoptotic population and FITC-Annexin V/PI double-positive cells indicate the necrotic population

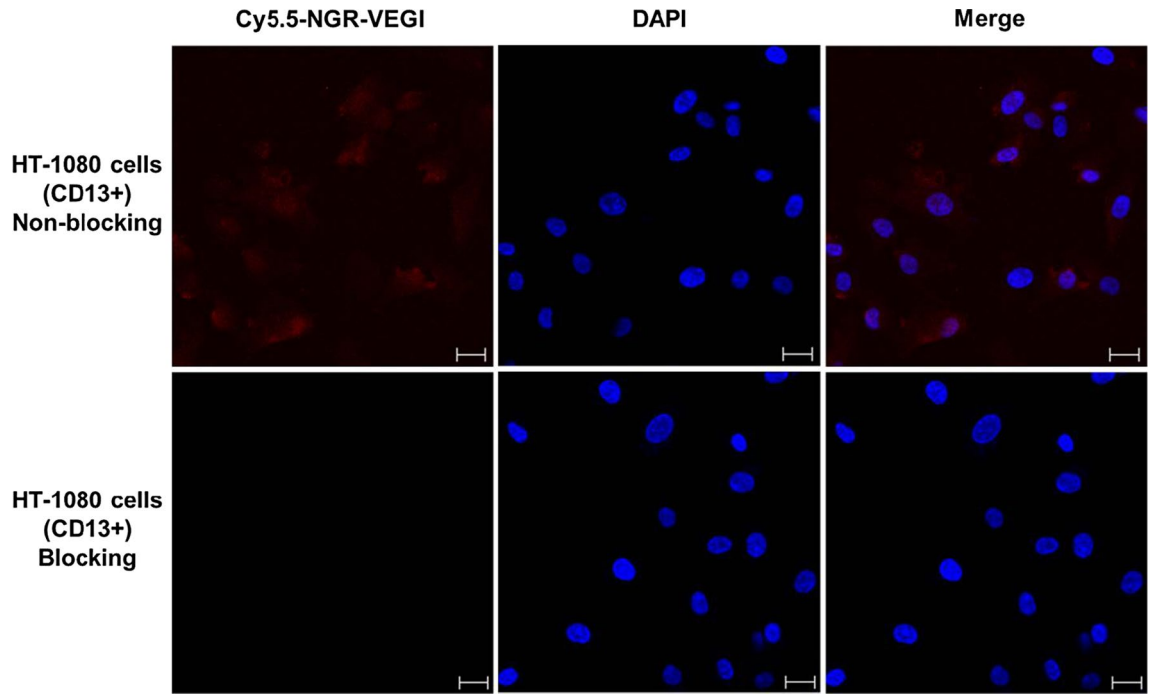

Fig. 5 Confocal microscopy results of Cy5.5-NGR–VEGI with HT-1080 cells (CD13 positive) (Magnification: 100×; *scale bar* 20 μm). The blocking study can be achieved by adding unlabeled NGR–VEGI protein. Top: Incubation of Cy5.5-NGR–VEGI (2 μM) with HT-1080 cells; Bottom: Incubation of Cy5.5-NGR–VEGI (2 μM) with HT-1080 cells blocked by unlabeled NGR–VEGI protein (2 mM)

Tumor-specific delivery of Cy5.5-NGR–VEGI monitored by in vivo fluorescence imaging

To ascertain the tumor-specific delivery of Cy5.5-NGR–VEGI, NIR fluorescence images of nude mice bearing subcutaneous HT-1080 tumor were acquired after intravenous injection of 1.5 nmol of Cy5.5-NGR–VEGI (Fig. 6a). Good contrast to background tissue of Cy5.5-NGR–VEGI in HT-1080 tumors can be visualized after 4 h pi, and highest tumor-to-background contrast was observed at 8 h pi. Fluorescence intensities in HT-1080 tumor and muscle were plotted as a function of time (Fig. 6b). The HT-1080 tumor uptake reached a maximum at 6 h pi and slowly washed out over time. In contrast, the normal tissue had faster probe binding and washout. The overall uptake of Cy5.5-NGR–VEGI in muscle was significantly lower as compared to HT-1080 tumor during 24 h study period.

The CD13 specificity of Cy5.5-NGR–VEGI was verified by a blocking experiment. For the blocking group, each HT-1080 tumor-bearing mouse was intravenously co-injected with 1.5 nmol of Cy5.5-NGR–VEGI and unlabeled NGR–VEGI (20 mg/kg), whereas mice in the non-blocking group were injected with 1.5 nmol of Cy5.5-NGR–VEGI only. The results showed that the unlabeled NGR–VEGI protein significantly reduced HT-1080 tumor uptake and tumor contrast at all imaging time points. The optical images of HT-1080 tumor-bearing mice at 8 h pi from the non-blocking and blocking group are presented in Fig. 7a. Tumor contrast as quantified by the ROI analysis of images indicated that the tumor-to-muscle value at 8 h pi was reduced from 14.98 ± 2.48 to 3.51 ± 0.85 ($P < 0.05$) (Fig. 7b).

Tumor-specific delivery of Cy5.5-NGR–VEGI confirmed by ex vivo fluorescence imaging

The results from ex vivo imaging were consistent with in vivo findings. Ex vivo evaluation of excised organs showed that Cy5.5-NGR–VEGI was predominantly taken up by the HT-1080 tumor at 8 h pi in the non-blocking group (Fig. 8a), as observed in the results of in vivo imaging. Aside from the HT-1080 tumor, liver uptake of Cy5.5-NGR–VEGI remained higher than the amounts measured in other major organs. Co-injection of Cy5.5-NGR–VEGI with unlabeled NGR–VEGI protein reduced the overall probe uptake, and the HT-1080 tumor uptake of Cy5.5-NGR–VEGI was not noticeable in the blocking group as compared to that in non-blocking group ($P < 0.05$) (Fig. 8b), suggesting the target specificity of Cy5.5-NGR–VEGI. Based on quantitative analysis of ex vivo imaging, the contrast ratios of tumor to normal

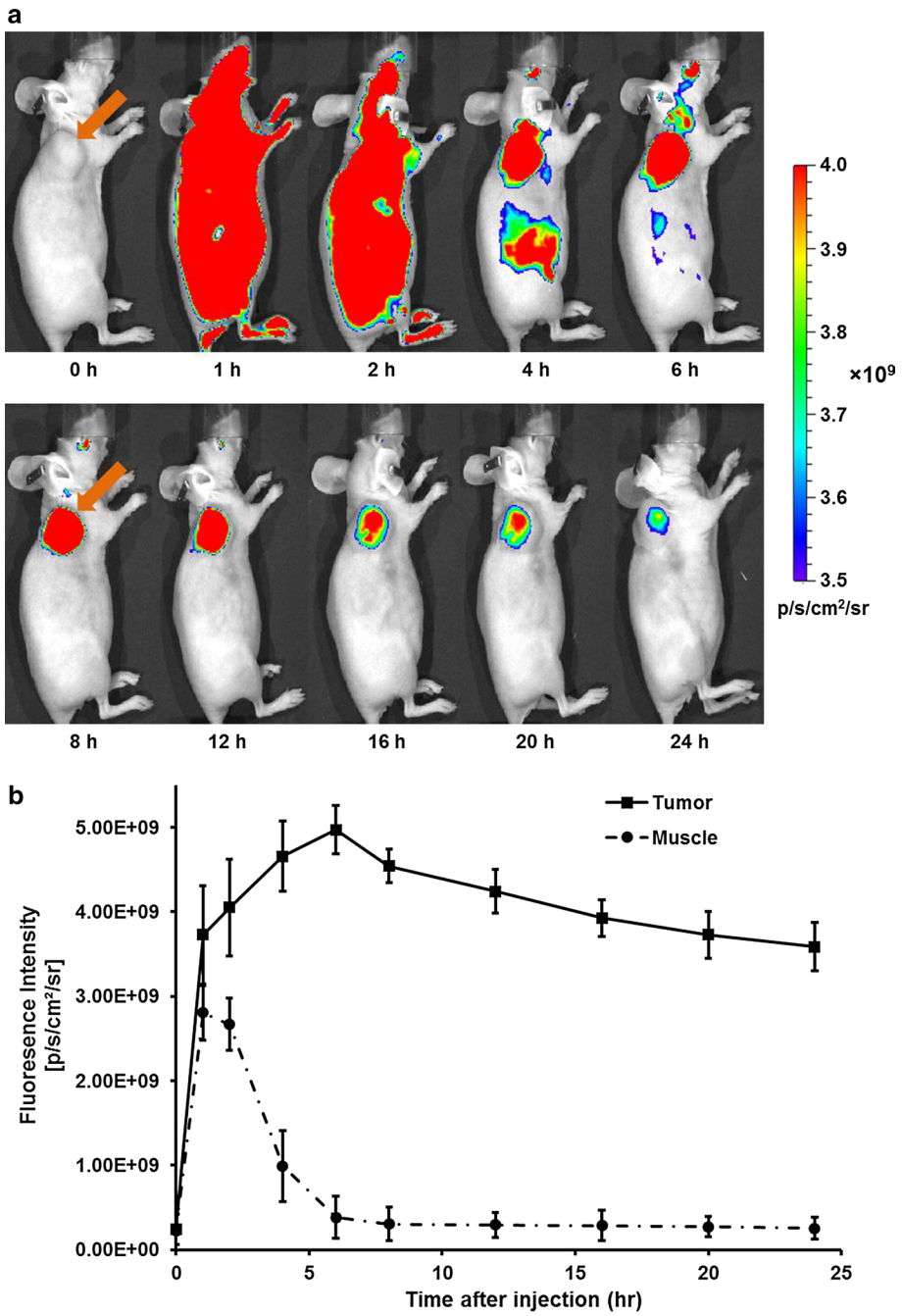

Fig. 6 **a** Time-course fluorescence imaging of subcutaneous HT-1080 tumor-bearing nude mice ($n = 6$) after intravenous injection of 1.5 nmol of Cy5.5-NGR–VEGI. The tumor can be clearly visualized as indicated by *arrows*. **b** Quantification and kinetics of in vivo targeting character of Cy5.5-NGR–VEGI in HT-1080 tumor vs. muscle. The Cy5.5-NGR–VEGI uptake in HT-1080 tumor at various time points was significantly higher than that in muscle. *Error bar* was calculated as the standard deviation ($n = 6$)

organs for non-blocking and blocking groups were calculated (Fig. 8c). The tumor-to-muscle ratio of Cy5.5-NGR–VEGI at 8 h pi in the non-blocking and blocking group was determined to be 18.93 ± 2.88 and 4.92 ± 0.75, respectively. In addition, the tumor-to-liver and tumor-to-kidney ratio of Cy5.5-NGR–VEGI at 8 h pi in the non-blocking group was calculated to be 0.86 ± 0.12 and 2.58 ± 0.34, respectively, whereas the corresponding values in the blocking group were 0.29 ± 0.35 and 0.86 ± 0.55, respectively.

Discussion

Near-infrared fluorescence optical imaging offers a noninvasive method for studying diseases at molecular level in living subjects (Kobayashi et al. 2010; Tung 2004; Weissleder and Mahmood 2001). As an excellent complement to nuclear imaging techniques, optical imaging, which uses neither ionizing radiation nor radioactive materials, is relatively inexpensive, highly sensitive, robust, and straightforward (Chen et al. 2004a). Recent advances in the field of molecular imaging

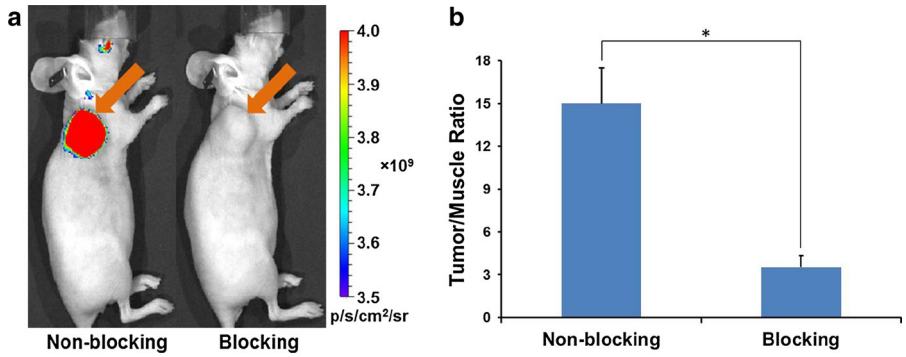

Fig. 7 **a** Representative fluorescence imaging (at 8 h pi) of mice bearing HT-1080 tumor on the right shoulder, demonstrating blocking of Cy5.5-NGR–VEGI (1.5 nmol) uptake by co-injection with NGR–VEGI (20 mg/kg). The tumors are indicated by *arrows*. **b** Fluorescence intensity ratio of tumor-to-muscle based on the ROI analysis. *Error bar* was calculated as the standard deviation ($n = 6$)

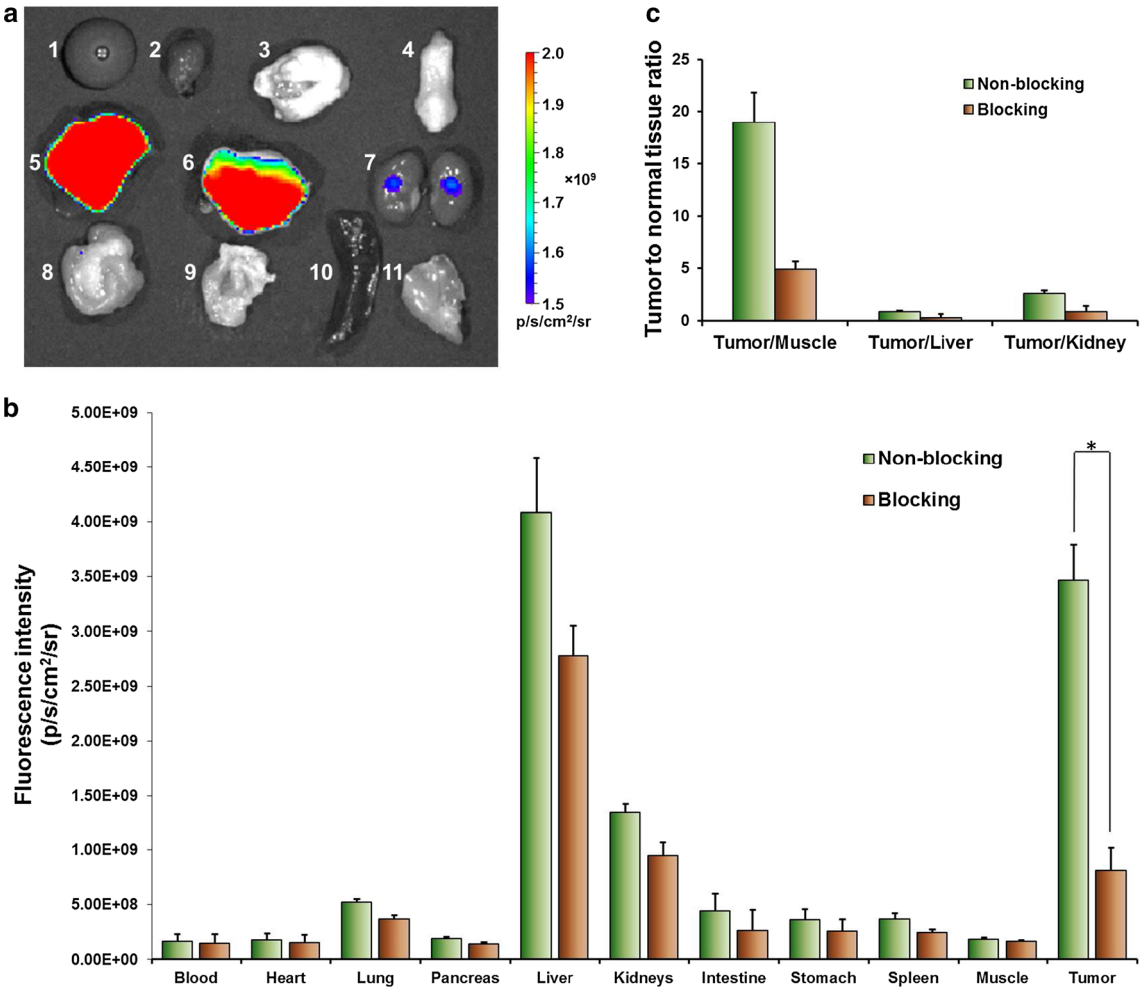

Fig. 8 **a** Ex vivo imaging of tumor and normal tissues of Cy5.5-NGR–VEGI after euthanizing the mice at 8 h pi; *1* Blood, *2* Heart, *3* Lung, *4* Pancreas, *5* Liver, *6* Tumor, *7* Kidneys, *8* Intestine, *9* Stomach, *10* Spleen, and *11* Muscle. **b** ROI analysis of ex vivo fluorescence intensity of major tissues with (blocking) and without (non-blocking) co-injection of NGR–VEGI protein (20 mg/kg). **c** Fluorescence intensity ratio of tumor-to-normal tissue based on the ROI analysis. *Error bar* was calculated as the standard deviation ($n = 3$)

have demonstrated that NIRF optical imaging can provide a unique opportunity to quantitatively evaluate the important biological targets, including cell surface receptors (Achilefu et al. 2000, 2002; Chen et al. 2004a; Cheng et al. 2005; Ke et al. 2003), intracellular enzymes (Mahmood and Weissleder 2003; Tung et al. 2004; Weissleder et al. 1999), and antigens (Moore et al. 2004). It is expected that NIRF optical imaging will make a significant impact in better understanding of the biology, early detection of disease, monitoring therapy response, and guiding drug discovery and development (Chen et al. 2012; Li et al. 2014; Zhang et al. 2013). For instance, bevacizumab, a humanized monoclonal antibody targeting VEGF, was conjugated to AlexaFluor 750 to provide the bevacizumab-AlexaFluor 750 probe (Paudyal et al. 2014). The optical imaging showed that bevacizumab-AlexaFluor 750 probe has great potential for noninvasive imaging of VEGF expression in HT29 colorectal cancer xenografts.

It has been documented that VEGI represents a potent endogenous inhibitor of angiogenesis. In endothelial cells, VEGI is usually functional to mediate two biological activities, i.e., (a) early G1 arrest in G0/G1 cells responding to growth stimuli, and (b) programmed death in proliferating cells (Yu et al. 2001). The ability of inducing apoptosis of endothelial cells by VEGI has been described as a putative mechanism through the activation of c-Jun N-terminal kinase (Haridas et al. 1999). Distinguishable splicing isoforms of VEGI have been discovered, namely, VEGI-174, VEGI-251, and VEGI-192, which differ in their N-terminal regions while sharing an identical C-terminal 151-residue segment (Hou et al. 2005; Zhai et al. 1999a). Chen et al. produced rhVEGI-192 with high yield, and demonstrated that the anti-angiogenic activity of rhVEGI-192 likely results from its capability of forming a polymeric structure (Chen et al. 2010). In addition, ectopic expression of VEGI-251 in tumor cells causes apoptosis of endothelial cells in tumor vasculature, reduction of microvessel density, and inhibition of tumor growth (Chew et al. 2002; Migone et al. 2002; Bamias et al. 2003). Overall, VEGI is one of the most promising anticancer agents through suppressing neovascularization. However, the limited source of natural VEGI prevents its translation into clinical studies. There is an increasing demand of developing the analogs of recombinant VEGI to fulfill this urgent medical need.

Theranostic biomaterials embrace the hope to propel the biomedical field toward personalized medicine by delivering diagnostic imaging agents and therapeutic drugs in one package. In our previous study, we developed several NGR-containing imaging probes which exhibit excellent binding affinity to CD13 receptor, a critical regulator of angiogenesis (Chen et al. 2013). The motivation of developing a theranostic biomaterial reserving biological features of both NGR peptide and VEGI protein leads us to the design of a fluorophore-containing NGR–VEGI fusion protein. In this study, we prepared a novel NGR–VEGI fusion protein from prokaryotic expression. Our data showed that the expression of NGR–VEGI protein must be induced by IPTG (Fig. 2). A predominant NGR–VEGI fusion protein can be detected as a single band with the expected molecular weight (21 kDa) using reducing SDS–PAGE. The biological function of newly prepared NGR–VEGI protein was determined based on the inhibition of HUVEC cell growth using flow cytometry analysis. As shown in Fig. 3, the treatment with NGR–VEGI protein resulted in the significant apoptosis of HUVEC, which was higher than that induced by the vector control, NGR peptide, and VEGI protein only. This result suggested that the newly developed NGR–VEGI fusion protein maintains the functionality of VEGI protein. We further demonstrated the in vivo therapeutic effect of NGR–VEGI fusion protein (unpublished data). To the best of our knowledge, our work is the first report on expression and purification of a biologically active NGR–VEGI fusion protein. After successfully obtaining the NGR–VEGI fusion protein, we conjugated the protein with a fluorescent Cy5.5 dye, a widely used and commercially available NIR probe. The newly constructed Cy5.5-NGR–VEGI protein exhibited good NIR property with the maximum absorption and emission wavelength at 673 nm and 693 nm, respectively (Fig. 4). Cy5.5-NGR–VEGI was then subjected to in vitro characterizations. The confocal microscopy results clearly demonstrated the target specificity of Cy5.5-NGR–VEGI. Interestingly, except for the cell surface binding, the intracellular localization of Cy5.5-NGR–VEGI in HT-1080 cells was also examined (Fig. 5). One possible explanation is that the fluorescence dye motif increases lipophilicity of the probe and thus facilitates ligand internalization. Nevertheless, the mechanism of cellular internalization of Cy5.5-NGR–VEGI requires further investigation.

To examine its tumor targeting efficacy, Cy5.5-NGR–VEGI was evaluated in the subcutaneous HT-1080 fibrosarcoma mouse xenografts. In vivo optical imaging studies showed that the Cy5.5-NGR–VEGI exhibited excellent tumor-to-background contrast at 8 h pi in the non-blocking group (Fig. 6). Cy5.5-NGR–VEGI also displayed decent tumor retention. The washout of Cy5.5-NGR–VEGI in tumor was much slower than normal tissues, leading to excellent tumor-to-normal tissue contrast between 8 and 20 h pi. A blocking experiment was achieved by co-injection of Cy5.5-NGR–VEGI with unlabeled NGR–VEGI protein (20 mg/kg). Significant reduced tumor uptake ($P < 0.05$) of Cy5.5-NGR–VEGI was observed for the blocking group vs. the non-blocking group at 8 h pi (Fig. 7), indicating Cy5.5-NGR–VEGI is a CD13-specific probe. Ex vivo NIRF imaging confirmed in vivo findings, showing that Cy5.5-NGR–VEGI was predominantly taken up by the HT-1080 tumor at 8 h pi in the non-blocking group (Fig. 8). The HT-1080 tumor uptake of Cy5.5-NGR–VEGI

in the blocking group was significantly lower than that in non-blocking group ($P < 0.05$), further suggesting the target specificity of Cy5.5-NGR–VEGI. Based on quantitative analysis of ex vivo imaging, the excellent tumor-to-muscle contrast ratio of Cy5.5-NGR–VEGI was calculated to be 18.93 ± 2.88 at 8 h pi.

Aside from the high HT-1080 tumor uptake, liver uptake of Cy5.5-NGR–VEGI was observed in ex vivo NIRF images, suggesting that the excretion route of Cy5.5-NGR–VEGI may be partially through the hepatic pathway. To further optimize the pharmacokinetics of NGR–VEGI protein, the liver uptake issue could conceivably be improved by appropriately incorporating hydrophilic elements into NGR–VEGI protein (Chen and Chen 2010). For example, Mario et al. performed chemical modifications of the most active VEGF-derived cyclopeptide (cyclo-VEGI). Hydrophilic linkers were synthesized and coupled to cyclo-VEGI. The results turned out that the chemical modifications enhanced the biological activity of cyclo-VEGI as measured in competition assays. In addition, ligand multimerization has been proved to be an effective approach by increasing the binding affinity of the ligand to its biological target and consequently reducing the non-specific binding of the ligand. For instance, others have reported that multimeric RGD peptide with repeating cyclic RGD units significantly enhanced the binding affinity of RGD ligand to integrin $\alpha_v\beta_3$ receptor due to multivalency effect (Chen et al. 2004b; Dijkgraaf et al. 2011; Jacobson et al. 2011). Recently, we also demonstrated that the binding affinity of dimeric NGR peptide to CD13 receptor is higher than that of monomeric NGR peptide (Chen et al. 2013; Westphal et al. 2013). The approach of employing multivalency effect enhances the "local ligand concentration" in the vicinity of the receptor, leading to a faster rate of receptor binding or a slower rate of dissociation of ligand from the target. In the future work, we may incorporate multimeric NGR units into the NGR–VEGI fusion protein to further enhance the target specificity of protein. Furthermore, our research plan also includes the development of NGR–VEGI containing nanoparticles (Xing et al. 2014). Based on the results demonstrated in this study, we envision that NGR–VEGI containing nanoparticles with large surface-to-volume ratio may offer new opportunities on developing novel NGR–VEGI based biomaterials for targeting tumor vasculature.

Conclusions

We successfully prepared a novel NGR–VEGI fusion protein, which offers improved functions for targeting tumor vasculature as compared to NGR peptide or VEGI protein. Our study further demonstrated that the specific delivery of NGR–VEGI protein in HT-1080 tumors can be longitudinally visualized and accurately quantified using NIRF imaging technique with a Cy5.5-labeled NGR–VEGI protein. As a novel theranostic protein, Cy5.5-NGR–VEGI has the potential to improve cancer treatment by targeting tumor vasculature.

Acknowledgments This work was supported by the USC Department of Radiology, the Major Program of National Natural Science Foundation of China (Grant No. 81230033), the National Basic Research and Development Program of China (Grant No. 2011CB707704), the Major Research Instrumentation Program of National Natural Science Foundation of China (Grant No. 81227901), the General Program of National Natural Science Foundation of China (Grant No. 81371594), and the International Cooperation Program of Xijing Hospital (Grant No. XJZT13G02).

Conflict of interest The authors declare that they have no conflict of interest.

References

Achilefu S, Dorshow RB, Bugaj JE, Rajagopalan R (2000) Novel receptor-targeted fluorescent contrast agents for in vivo tumor imaging. Invest Radiol 35(8):479–485

Achilefu S, Jimenez HN, Dorshow RB, Bugaj JE, Webb EG, Wilhelm RR, Rajagopalan R, Johler J, Erion JL (2002) Synthesis, in vitro receptor binding, and in vivo evaluation of fluorescein and carbocyanine peptide-based optical contrast agents. J Med Chem 45(10):2003–2015

Balkwill F, Charles KA, Mantovani A (2005) Smoldering and polarized inflammation in the initiation and promotion of malignant disease. Cancer Cell 7(3):211–217

Bamias G, Martin C 3rd, Marini M, Hoang S, Mishina M, Ross WG, Sachedina MA, Friel CM, Mize J, Bickston SJ, Pizarro TT, Wei P, Cominelli F (2003) Expression, localization, and functional activity of TL1A, a novel Th1-polarizing cytokine in inflammatory bowel disease. J Immunol 171(9):4868–4874

Bhagwat SV, Lahdenranta J, Giordano R, Arap W, Pasqualini R, Shapiro LH (2001) CD13/APN is activated by angiogenic signals and is essential for capillary tube formation. Blood 97(3):652–659

Carmeliet P (2005) Angiogenesis in life, disease and medicine. Nature 438(7070):932–936

Chen K, Chen X (2010) Design and development of molecular imaging probes. Curr Top Med Chem 10(12):1227–1236

Chen K, Chen X (2011) Positron emission tomography imaging of cancer biology: current status and future prospects. Semi Oncol 38(1):70–86

Chen K, Conti PS (2010) Target-specific delivery of peptide-based probes for PET imaging. Adv Drug Deliv Rev 62(11):1005–1022

Chen X, Conti PS, Moats RA (2004a) In vivo near-infrared fluorescence imaging of integrin $\alpha_V\beta_3$ in brain tumor xenografts. Cancer Res 64(21):8009–8014

Chen X, Tohme M, Park R, Hou Y, Bading JR, Conti PS (2004b) Micro-PET imaging of $\alpha_V\beta_3$-integrin expression with ^{18}F-labeled dimeric RGD peptide. Mol Imaging 3(2):96–104

Chen X, Wu J, Liu H, He Z, Gu M, Wang N, Ma J, Hu J, Xia L, He H, Yuan J, Li J, Li L, Li M, Zhu X (2010) Approaches to efficient production of recombinant angiogenesis inhibitor rhVEGI-192 and characterization of its structure and antiangiogenic function. Protein Sci 19(3):449–457

Chen K, Yap LP, Park R, Hui X, Wu K, Fan D, Chen X, Conti PS (2012) A Cy5.5-labeled phage-displayed peptide probe for

near-infrared fluorescence imaging of tumor vasculature in living mice. Amino Acids 42(4):1329–1337

Chen K, Ma W, Li G, Wang J, Yang W, Yap LP, Hughes LD, Park R, Conti PS (2013) Synthesis and evaluation of ^{64}Cu-labeled monomeric and dimeric NGR peptides for MicroPET imaging of CD13 receptor expression. Mol Pharm 10(1):417–427

Cheng Z, Wu Y, Xiong Z, Gambhir SS, Chen X (2005) Near-infrared fluorescent RGD peptides for optical imaging of integrin $\alpha_V\beta_3$ expression in living mice. Bioconjugate Chem 16(6):1433–1441

Chew LJ, Pan H, Yu J, Tian S, Huang WQ, Zhang JY, Pang S, Li LY (2002) A novel secreted splice variant of vascular endothelial cell growth inhibitor. FASEB J 16(7):742–744

Coussens LM, Werb Z (2002) Inflammation and cancer. Nature 420(6917):860–867

Dijkgraaf I, Yim CB, Franssen GM, Schuit RC, Luurtsema G, Liu S, Oyen WJ, Boerman OC (2011) PET imaging of $\alpha_V\beta_3$ integrin expression in tumours with ^{68}Ga-labelled mono-, di- and tetrameric RGD peptides. Eur J Nucl Med Mol Imaging 38(1):128–137

Duan L, Yang G, Zhang R, Feng L, Xu C (2012) Advancement in the research on vascular endothelial growth inhibitor (VEGI). Target Oncol 7(1):87–90

Folkman J (1971) Tumor angiogenesis: therapeutic implications. N Engl J Med 285(21):1182–1186

Folkman J (2006) Angiogenesis. Annu Rev Med 57:1–18

Goncalves M, Estieu-Gionnet K, Berthelot T, Lain G, Bayle M, Canron X, Betz N, Bikfalvi A, Deleris G (2005) Design, synthesis, and evaluation of original carriers for targeting vascular endothelial growth factor receptor interactions. Pharm Res 22(8):1411–1421

Guzman-Rojas L, Rangel R, Salameh A, Edwards JK, Dondossola E, Kim YG, Saghatelian A, Giordano RJ, Kolonin MG, Staquicini FI, Koivunen E, Sidman RL, Arap W, Pasqualini R (2012) Cooperative effects of aminopeptidase N (CD13) expressed by nonmalignant and cancer cells within the tumor microenvironment. Proc Natl Acad Sci USA 109(5):1637–1642

Hanahan D, Folkman J (1996) Patterns and emerging mechanisms of the angiogenic switch during tumorigenesis. Cell 86(3):353–364

Haridas V, Shrivastava A, Su J, Yu GL, Ni J, Liu D, Chen SF, Ni Y, Ruben SM, Gentz R, Aggarwal BB (1999) VEGI, a new member of the TNF family activates nuclear factor-kappa B and c-Jun N-terminal kinase and modulates cell growth. Oncogene 18(47):6496–6504

Hou W, Medynski D, Wu S, Lin X, Li LY (2005) VEGI-192, a new isoform of TNFSF15, specifically eliminates tumor vascular endothelial cells and suppresses tumor growth. Clin Cancer Res 11(15):5595–5602

Jacobson O, Zhu L, Ma Y, Weiss ID, Sun X, Niu G, Kiesewetter DO, Chen X (2011) Rapid and simple one-step F-18 labeling of peptides. Bioconjugate Chem 22(3):422–428

Ke S, Wen X, Gurfinkel M, Charnsangavej C, Wallace S, Sevick-Muraca EM, Li C (2003) Near-infrared optical imaging of epidermal growth factor receptor in breast cancer xenografts. Cancer Res 63(22):7870–7875

Kelkar SS, Reineke TM (2011) Theranostics: combining imaging and therapy. Bioconjugate Chem 22(10):1879–1903

Kobayashi H, Ogawa M, Alford R, Choyke PL, Urano Y (2010) New strategies for fluorescent probe design in medical diagnostic imaging. Chem Rev 110(5):2620–2640

Li G, Xing Y, Wang J, Conti PS, Chen K (2014) Near-infrared fluorescence imaging of CD13 receptor expression using a novel Cy5.5-labeled dimeric NGR peptide. Amino Acids 46(6):1547–1556

Lopez-Otin C, Matrisian LM (2007) Emerging roles of proteases in tumour suppression. Nature Rev Cancer 7(10):800–808

Mahmood U, Weissleder R (2003) Near-infrared optical imaging of proteases in cancer. Mol Cancer Ther 2(5):489–496

Meng J, Yan Z, Wu J, Li L, Xue X, Li M, Li W, Hao Q, Wan Y, Qin X, Zhang C, You Y, Han W, Zhang Y (2007) High-yield expression, purification and characterization of tumor-targeted IFN-alpha2a. Cytotherapy 9(1):60–68

Migone TS, Zhang J, Luo X, Zhuang L, Chen C, Hu B, Hong JS, Perry JW, Chen SF, Zhou JX, Cho YH, Ullrich S, Kanakaraj P, Carrell J, Boyd E, Olsen HS, Hu G, Pukac L, Liu D, Ni J, Kim S, Gentz R, Feng P, Moore PA, Ruben SM, Wei P (2002) TL1A is a TNF-like ligand for DR3 and TR6/DcR3 and functions as a T cell costimulator. Immunity 16(3):479–492

Moore A, Medarova Z, Potthast A, Dai G (2004) In vivo targeting of underglycosylated MUC-1 tumor antigen using a multimodal imaging probe. Cancer Res 64(5):1821–1827

Parr C, Gan CH, Watkins G, Jiang WG (2006) Reduced vascular endothelial growth inhibitor (VEGI) expression is associated with poor prognosis in breast cancer patients. Angiogenesis 9(2):73–81

Pasqualini R, Koivunen E, Kain R, Lahdenranta J, Sakamoto M, Stryhn A, Ashmun RA, Shapiro LH, Arap W, Ruoslahti E (2000) Aminopeptidase N is a receptor for tumor-homing peptides and a target for inhibiting angiogenesis. Cancer Res 60(3):722–727

Paudyal B, Paudyal P, Shah D, Tominaga H, Tsushima Y, Endo K (2014) Detection of vascular endothelial growth factor in colon cancer xenografts using bevacizumab based near infrared fluorophore conjugate. J Biomed Sci 21:35

Petrovic N, Schacke W, Gahagan JR, O'Conor CA, Winnicka B, Conway RE, Mina-Osorio P, Shapiro LH (2007) CD13/APN regulates endothelial invasion and filopodia formation. Blood 110(1):142–150

Risau W (1997) Mechanisms of angiogenesis. Nature 386(6626):671–674

Sacchi A, Gasparri A, Curnis F, Bellone M, Corti A (2004) Crucial role for interferon gamma in the synergism between tumor vasculature-targeted tumor necrosis factor alpha (NGR-TNF) and doxorubicin. Cancer Res 64(19):7150–7155

Studier FW (2005) Protein production by auto-induction in high density shaking cultures. Protein Expr Purif 41(1):207–234

Tung CH (2004) Fluorescent peptide probes for in vivo diagnostic imaging. Biopolymers 76(5):391–403

Tung CH, Zeng Q, Shah K, Kim DE, Schellingerhout D, Weissleder R (2004) In vivo imaging of beta-galactosidase activity using far red fluorescent switch. Cancer Res 64(5):1579–1583

von Wallbrunn A, Waldeck J, Holtke C, Zuhlsdorf M, Mesters R, Heindel W, Schafers M, Bremer C (2008) In vivo optical imaging of CD13/APN-expression in tumor xenografts. J Biomed Opt 13(1):011007

Weissleder R (2006) Molecular imaging in cancer. Science 312(5777):1168–1171

Weissleder R, Mahmood U (2001) Molecular imaging. Radiology 219(2):316–333

Weissleder R, Tung CH, Mahmood U, Bogdanov A Jr (1999) In vivo imaging of tumors with protease-activated near-infrared fluorescent probes. Nat Biotechnol 17(4):375–378

Westphal M, Yla-Herttuala S, Martin J, Warnke P, Menei P, Eckland D, Kinley J, Kay R, Ram Z (2013) Adenovirus-mediated gene therapy with sitimagene ceradenovec followed by intravenous ganciclovir for patients with operable high-grade glioma (ASPECT): a randomised, open-label, phase 3 trial. Lancet Oncol 14(9):823–833

Xiao Q, Hsu CY, Chen H, Ma X, Xu J, Lee JM (2005) Characterization of cis-regulatory elements of the vascular endothelial growth inhibitor gene promoter. Biochem J 388(Pt 3):913–920

Xing Y, Zhao J, Conti PS, Chen K (2014) Radiolabeled nanoparticles for multimodality tumor imaging. Theranostics 4(3):290–306

Yu J, Tian S, Metheny-Barlow L, Chew LJ, Hayes AJ, Pan H, Yu GL, Li LY (2001) Modulation of endothelial cell growth arrest and apoptosis by vascular endothelial growth inhibitor. Circ Res 89(12):1161–1167

Zhai Y, Ni J, Jiang GW, Lu J, Xing L, Lincoln C, Carter KC, Janat F, Kozak D, Xu S, Rojas L, Aggarwal BB, Ruben S, Li LY, Gentz R, Yu GL (1999a) VEGI, a novel cytokine of the tumor necrosis factor family, is an angiogenesis inhibitor that suppresses the growth of colon carcinomas in vivo. FASEB J 13(1):181–189

Zhai Y, Yu J, Iruela-Arispe L, Huang WQ, Wang Z, Hayes AJ, Lu J, Jiang G, Rojas L, Lippman ME, Ni J, Yu GL, Li LY (1999b) Inhibition of angiogenesis and breast cancer xenograft tumor growth by VEGI, a novel cytokine of the TNF superfamily. Int J Cancer 82(1):131–136

Zhang Z, Harada H, Tanabe K, Hatta H, Hiraoka M, Nishimoto S (2005) Aminopeptidase N/CD13 targeting fluorescent probes: synthesis and application to tumor cell imaging. Peptides 26(11):2182–2187

Zhang N, Sanders AJ, Ye L, Jiang WG (2009a) Vascular endothelial growth inhibitor in human cancer (Review). Int J Mol Med 24(1):3–8

Zhang N, Sanders AJ, Ye L, Kynaston HG, Jiang WG (2009b) Vascular endothelial growth inhibitor, expression in human prostate cancer tissue and the impact on adhesion and migration of prostate cancer cells in vitro. Int J Oncol 35(6):1473–1480

Zhang N, Sanders AJ, Ye L, Kynaston HG, Jiang WG (2010) Expression of vascular endothelial growth inhibitor (VEGI) in human urothelial cancer of the bladder and its effects on the adhesion and migration of bladder cancer cells in vitro. Anticancer Res 30(1):87–95

Zhang S, Shao P, Bai M (2013) In vivo type 2 cannabinoid receptor-targeted tumor optical imaging using a near infrared fluorescent probe. Bioconjugate Chem 24(11):1907–1916